The Intra-Americas Springtime Sea Surface Temperature Anomaly Dipole as Fingerprint of Remote Influences

Ernesto Muñoz

Cooperative Institute for Marine and Atmospheric Studies, Rosenstiel School for Marine and Atmospheric Science, University of Miami, Miami, Florida

Chunzai Wang

National Oceanic and Atmospheric Administration/Atlantic Oceanographic and Meteorological Laboratory, Miami, Florida

David Enfield

Cooperative Institute for Marine and Atmospheric Studies, Rosenstiel School for Marine and Atmospheric Science, University of Miami, Miami, Florida

(Manuscript received 5 January 2009, in final form 13 July 2009)

ABSTRACT

The influence of teleconnections on the Intra-Americas Sea (IAS; Gulf of Mexico and Caribbean Sea) has been mostly analyzed from the perspective of El Niño–Southern Oscillation (ENSO) on the Caribbean Sea (the latter being an extension of the tropical North Atlantic). This emphasis has overlooked both 1) the influence of other teleconnections on the IAS and 2) which teleconnections affect the Gulf of Mexico climate variability. In this study the different fingerprints that major teleconnection patterns have on the IAS during boreal spring are analyzed. Indices of teleconnection patterns are regressed and correlated to observations of oceanic temperature and atmospheric data from reanalyses and observational datasets. It is found that the Pacific teleconnection patterns that influence the IAS SSTs do so by affecting the Gulf of Mexico in an opposite manner to the Caribbean Sea. These analyzed Pacific climate patterns are the Pacific–North American (PNA) teleconnection, the Pacific decadal oscillation (PDO), and ENSO. The North Atlantic Oscillation (NAO) is related to a lesser degree with the north–south SST anomaly dipole than are Pacific teleconnection patterns. It is also found that the IAS influence from the midlatitude Pacific mostly affects the Gulf of Mexico, whereas the influence from the tropical Pacific mostly affects the Caribbean Sea. Therefore, the combination of a warm ENSO event and a positive PNA event induces a strong IAS SST anomaly dipole between the Gulf of Mexico and the Caribbean Sea during spring.

By calculating an index that represents the IAS SST anomaly dipole, it is found that the dipole forms mostly in response to changes in the air–sea heat fluxes. In the Gulf of Mexico the dominant mechanisms are the air–sea differences in humidity and temperature. The changes in shortwave radiation also contribute to the dipole of net air–sea heat flux. The changes in shortwave radiation arise, in part, by the cloudiness triggered by the air–sea differences in humidity, and also by the changes in the convection cell that connects the Amazon basin to the IAS. Weaker Amazon convection (e.g., in the event of a warm ENSO event) reduces the subsidence over the IAS, and henceforth the IAS cloudiness increases (and the shortwave radiation decreases). This study contributes to a greater understanding of how the IAS is influenced by different Pacific and Atlantic teleconnections.

1. Introduction

In addition to Atlantic influence, the springtime tropical North Atlantic (TNA) sea surface temperature anomalies

(SSTAs) are remotely forced by tropical Pacific SSTAs, in particular anomalies related to El Niño–Southern Oscillation (ENSO; Enfield and Mayer 1997; Saravanan and Chang 2000). Enfield and Mayer (1997) observed that in response to wintertime Pacific warm ENSO events, the TNA SSTAs warm up during boreal spring as a result of the weakening of the North Atlantic subtropical high (NASH) and the associated easterlies. The weakening

Corresponding author address: Ernesto Muñoz, 4600 Rickenbacker Causeway, CIMAS/RSMAS, University of Miami, Miami, FL 33149. E-mail: ernesto.munoz@noaa.gov

of the TNA low-level easterlies, including those in the Caribbean Sea, results in a decreased latent heat loss that warms the ocean mixed layer (Alexander and Scott 2002) and a decreased mixing of mixed layer water with cooler subsurface water (Enfield and Mayer 1997). Additionally, during the month of January, the air–sea difference in humidity contributes to the latent heat flux anomalies in the Caribbean Sea (Chikamoto and Tanimoto 2005). In the Gulf of Mexico, changes in the subtropical jet and the storm tracks associated with ENSO may affect the moisture availability (Coleman and Rogers 2007). It is known that with El Niño (La Niña), the storm tracks and frontal passages are displaced farther south (north) along the gulf coast (Compo and Sardeshmukh 2004; Eichler and Higgins 2006).

Together, the Caribbean Sea (CBN) and Gulf of Mexico (GMX) are called the Intra-Americas Sea (IAS). However, the focus of many previous studies has been on the relation of ENSO to TNA SSTAs. The factors related to the Gulf of Mexico SSTAs have been comparatively understudied. Because springtime forcing of the ocean mixed layer is critical to the development of summer warm pool anomalies, an improved understanding of the processes during spring is desirable. Furthermore, questions remain as to what other teleconnections (aside from ENSO) influence the IAS climate variability during early spring. Several studies have analyzed the IAS variability in summer and its impact (e.g., Muñoz et al. 2008; Wang et al. 2008). However, IAS forcing during boreal spring is a critical factor in determining the size and intensity of the summer Atlantic warm pool (Enfield et al. 2006; Lee et al. 2008), which in turn influences rainfall and tropical cyclones during the ensuing summer (Wang et al. 2008).

Also relevant to the IAS is the Pacific–North American (PNA) pattern, which has an extension over the Florida peninsula that may influence the IAS climate anomalies. At longer time scales, the Pacific decadal oscillation (PDO) is another Pacific mode of variability that could influence the IAS because it has been observed to influence temperature and precipitation over northern South America (Dettinger et al. 2001; Mantua and Hare 2002). A complicating factor is that the Pacific climate modes are not fully orthogonal to each other; ENSO is correlated in time with the PNA and spatially with the PDO. Hence, attempts to separate their respective impacts on IAS SSTAs must be pursued with caution.

Changes in the Amazon convection may also influence the IAS during boreal spring. During this time Amazon convection is part of the atmospheric meridional overturning circulation that has a sinking branch over the tropical and subtropical North Atlantic, and its changes may in turn be reflected in the TNA atmosphere. The changes in convection over the Amazon

have been explained as a response to subsidence and stabilization of the upper troposphere (Lintner and Chiang 2007) as well as to changes in diabatic heating resulting from other factors (e.g., Koren et al. 2004). The Amazon convection is subject to the influence of ENSO anomalies and may be another conduit by which ENSO events affect the TNA atmosphere (Mestas-Nuñez and Enfield 2001; Wang 2002, 2004; Chiang and Sobel 2002).

The North Atlantic Oscillation (NAO) is another major teleconnection mechanism of the Northern Hemisphere winter and whose influence may extend into the spring season. However, its nature has been ascribed to either atmospheric internal variability or forced Atlantic SSTs (Czaja and Frankignoul 2002; Okumura et al. 2001). Paeth et al. (2003) finds that at intraseasonal time scales the NAO drives the North Atlantic SSTs but at longer time scales the North Atlantic SSTs drive the NAO.

The North Atlantic SSTAs show rich structures during boreal winter and spring. Deser and Timlin (1997) observed the dominant wintertime SSTA pattern at the intraseasonal time scale to be a SSTA tripole with positive nodes in the TNA (south of about 20°N) and in the high-latitude North Atlantic (between 45° and 65°N) opposing a middle antinode off the east coast of the United States. Tanimoto and Xie (2002) observed a similar pattern at the decadal time scale. In one phase, this North Atlantic tripole is reflected in the IAS as a dipole with positive SSTAs in the Caribbean Sea and negative SSTAs in the Gulf of Mexico (merging into the east coast antinode). Additionally, the IAS dipole has been observed in the spring following strong ENSO events (Alexander and Scott 2002; Wang et al. 2004; Chikamoto and Tanimoto 2005) and in the spring prior to anomalously large or small summer Western Hemisphere warm pools (Enfield et al. 2006). Some studies report a north–south dipole pattern of cloudiness and shortwave radiation anomalies over the IAS associated with ENSO (Curtis and Hastenrath 1995; Klein et al. 1999; Lau and Nath 2001). The IAS SSTA dipole, however, has been an overlooked feature of the IAS variability and merits further study.

In this study we analyze the IAS SSTA dipole between the Caribbean Sea and the Gulf of Mexico during late winter and early spring. Furthermore, we focus on the teleconnections to the IAS based on the SSTA dipole.

2. Data

To capture the IAS SSTA dipole, the extended reconstructed SST, version 3 (ERSST.v3) data (Smith et al. 2008) were used for the period 1949–2006. Based on the Comprehensive Ocean–Atmosphere Data Set (COADS) from 1945 to 1993 (Woodruff et al. 1987) and the International COADS from 1960 to 2002, Wang

et al. (2006) derived a dataset that was interpolated to a regular grid of 1° latitude × 1° longitude. From this derived dataset, the 1949–2002 turbulent and radiative heat fluxes between the air and the sea and surface wind stress and its curl were used. Other atmospheric fields analyzed here include precipitation from the University of Delaware (Willmott and Matsuura 2007), and 250-hPa velocity potential and 500-hPa vertical pressure velocity from the National Centers for Environmental Prediction–National Center for Atmospheric Research (NCEP–NCAR) reanalysis (Kalnay et al. 1996). The Simple Ocean Data Assimilation (SODA; Carton and Giese 2008) is an ocean reanalysis dataset with velocity, salinity, and temperature at various depths. The version of the SODA used for this study was version 2.0.2 and was analyzed in the context of the subsurface anomalies related to the IAS dipole. For all of the variables mentioned above, monthly anomalies were obtained by subtracting the 1971–2000 climatologies.

The COADS-derived heat fluxes are displayed following the convention that the net heat flux (Qnet, positive downward) is computed as Qnet = SW − LW − LH − SH, where SW is shortwave radiation, LW is longwave radiation, LH is latent heat flux, and SH is sensible heat flux, and fluxes are positive into the ocean. The bulk formulas for turbulent heat fluxes are dependent on the wind speed (W), and the air–sea difference of humidity δq (for LH) and temperature δT (for SH). These formulas can be decomposed into their time mean and deviation from the mean (′) to obtain SH = $c(W'\delta T + W\delta T')$ and LH = $c(W'\delta q + W\delta q')$, where c is a nondimensional constant. The flux decomposition neglects the nonlinear terms ($W'\delta T'$ or $W'\delta q'$) that are smaller. The decompositions of the turbulent heat fluxes were regressed onto the dipole index.

Teleconnection indices were obtained from the National Oceanic and Atmospheric Administration/Climate Prediction Center (NOAA/CPC) and Earth System Research Laboratory (ESRL) Web sites. The following indices were used for these analyses: the PNA pattern, the Niño-3.4 SSTA index, the equatorial Southern Oscillation index (EQSOI), the PDO index, and the NAO index. The Pacific meridional mode (PMM) index (Chiang and Vimont 2004) was also used. The Atlantic Multidecadal Oscillation (AMO) index was derived by averaging the detrended SSTAs in the North Atlantic region (Enfield et al. 2001). The anomalies were calculated based on the 1951–80 climatology, detrended by calendar month (based on the 1860–2002 trend) and smoothed with an 11-yr low-pass filter. Finally, the smoothed and detrended SSTAs were averaged from 5° to 65°N and from the eastern boundary (excluding the Mediterranean Sea) to the western boundary of the Atlantic (including the Gulf of Mexico) to obtain the AMO index. A similar SSTA area index, but for the 11-yr high-pass anomalies, was also calculated.

Considering the relation between the PNA and ENSO, we calculate the correlation between the PNA and Niño-3.4 indices used here. Even though the PNA has been described as the midlatitude manifestation of the ENSO signal (Wallace and Gutzler 1981), there is only a moderate correlation between these two indices. The concurrent correlation between the Niño-3.4 and PNA indices is highest during March, with a significant correlation of 0.48. The lagged correlation is highest whenever the March PNA index is used (e.g., Niño-3.4 in January and PNA in March) but is still below 0.45. The correlation throughout the rest of the winter and spring months (December–February and April) is between 0.30 and 0.24. This low correlation is not surprising given that some studies have identified the PNA and ENSO as separate modes of variability during winter (Rodionov and Assel 2001; Nigam 2003) and early spring. That is, the PNA is an internal mode of atmospheric variability whose rate of occurrence is either modestly or not affected by remote forcing from ENSO (Trenberth et al. 1998; Straus and Shukla 2002). The PDO, however, correlates more highly with the PNA. From January through April the correlation of the PDO and the PNA (0.58) is greater than that between the PDO and Niño-3.4 (0.44). However, the significant levels between these correlations are different because the decorrelation time scale of the Niño-3.4 index is shorter than the decorrelation time scale of the PDO index. After calculating the effective correlation [by taking into account the autocorrelation of each of the indices; see Sciremammano (1979)], the correlation between the PDO and the Niño-3.4 is 3.8 times their effective correlation, and that between the PDO and the PNA is 3.55 times their effective correlation, indicating a slightly stronger correlation between the PDO and the Niño-3.4 indices.

3. The IAS dipole

The correlation between SSTAs in the Gulf of Mexico and in the Caribbean Sea for the different seasons shows a cycle with negative correlation that peaks in late winter and early spring and positive correlations that peak in late summer and early fall (Table 1). The CBN SSTA index was constructed by averaging the SSTAs in the domain of 12°–20°N, 66°–88°W. For the GMX index, the SSTAs were averaged within 22°–32°N, 76°–96°W. The Pacific was not included when calculating the area averages. To determine whether an SSTA dipole in the IAS is statistically significant, we quantify the chi-square statistic from a contingency table. Data for the month of March were used. A contingency table and the derived statistic are used to analyze the degree of independence

TABLE 1. Seasonal correlation between SSTAs in the Gulf of Mexico and in the Caribbean Sea. The Caribbean area average is 12°–20°N, 66°–88°W, and the Gulf of Mexico area average is 22°–32°N, 76°–96°W, excluding the Pacific data.

Season	Correlation coefficient
November–January	−0.16
February–April	−0.44
May–July	0.31
August–October	0.54

TABLE 2. Contingency table for instances when the SSTAs in GMX and CBN fall in their extreme tercile ranges or intertercile range. The chi-square statistic is 19.43, with 4 degrees of freedom.

	GMX < Tt	|GMX| < Tt	GMX > Tt	Total
CBN > Tt	10	4	8	22
|CBN| < Tt	7	11	2	20
CBN < Tt	0	5	11	16
Total	17	20	21	58

of two variables. Contingency tables have been used, for example, in the context of the tropical Atlantic dipole (interhemispheric mode) by Enfield et al. (1999). For the present study, the two variables were the Caribbean SSTAs and the Gulf of Mexico SSTAs.

The contingency table was constructed using terciles of the CBN and GMX indices for the 58 yr from 1949 to 2006. Table 2 shows the number of cases in each category. The contingency table statistics were computed with the VassarStats Web site for Statistical Computation [available online at http://faculty.vassar.edu/lowry/VassarStats.html]. For the present combinations there are 4 degrees of freedom and the chi-square statistic at the 5% level of significance should be greater than 9.49 to reject the null hypothesis that the CBN SSTAs are independent of the GMX SSTAs. The expected frequency was greater than five for more than 80% of the table cells, which renders the chi-square statistic valid. For the contingency table, the chi-square statistic was 19.53 and the null hypothesis is rejected. This indicates that the table shows contingency between the two variables and that the CBN and GMX SSTAs are not independent, their relation being one of opposition to each other.

Next, we calculate an IAS SSTA dipole index and analyze it with respect to the climate anomalies related to it. The IAS SSTA dipole index was calculated as the difference of March SST standardized anomalies in the Caribbean minus those from the Gulf of Mexico for those years in which the SSTAs in either basin are of an opposite sign to those of the other basin. To identify the dipole years we construct a mask that takes into consideration the difference and sum of the CBN and GMX indices with the following formula: abs[(CBN − GMX)/(CBN + GMX)] − 1.0. The years for which the mask is less than zero are not taken into account in the dipole index and are categorized as nondipole years. The CBN and GMX SSTA indices for the dipole years and the nondipole years are presented in Fig. 1. The IAS dipole index results in a time series with small-to-large IAS dipoles that are symmetrical in some years and dominated by either basin in others.

Figure 2 shows the correlation between the IAS SSTA dipole index and SSTAs from February to April. The

nondipole years were not included and therefore the degrees of freedom were estimated by the number of dipole years minus one. The dipole is evident with cold SSTAs in the Gulf of Mexico and opposing SSTAs in the Caribbean Sea. The Caribbean Sea SSTAs are part of a larger anomalous SSTA pattern that crosses the TNA from the east to the west. [In the tropical South Atlantic (TSA), however, there are no SSTAs, suggesting that the IAS dipole may not be related to TSA variability.] The Gulf of Mexico SSTAs are also related to anomalies that extend to the east until about 40°W and to the north. Corroboration of the SSTA dipole was done with other datasets such as the Hadley Centre Global Sea Ice and Sea Surface Temperature (HadISST; Rayner et al. 2006) and SODA (Carton and Giese 2008). The statistically significant SSTAs in the Pacific and Indian Oceans are an indication that the dipole is related to teleconnections.

The atmospheric low-level circulation anomalies associated with the dipole are shown in Fig. 3. There are cyclonic anomalies in the midlatitude North Atlantic and also in the higher latitudes of the North Pacific (the Aleutian low region). These are separated by moderate pressure anomalies over the North American continent. Consequently, the 850-hPa wind over the IAS weakens with respect to the normal flow over the GMX (southerly) and CBN (easterly). In the tropical Pacific the westerly wind anomalies corresponding to a warm ENSO event can also be appreciated. In the midlatitude Pacific the North Pacific node of the PNA pattern stands out.

Figure 4 shows the correlation coefficients between several teleconnection indices and the IAS dipole index. In March, the dipole is highly correlated with several teleconnection indices including Niño-3.4 ($r = 0.71$), the PNA ($r = 0.58$), and the PDO ($r = 0.66$). However, although statistically significant, the correlation with the NAO ($r = -0.37$) is not as high as that with the Pacific indices. The AMO index calculated for this study has a low correlation ($r < 0.10$) with the dipole index, but the 11-yr high-pass North Atlantic SSTA index is highly correlated with the dipole index.

Shown in Fig. 5 are the SST anomalies associated with the two North Atlantic SSTA indices [the low-pass (AMO) and the high-pass indices]. The low-pass index
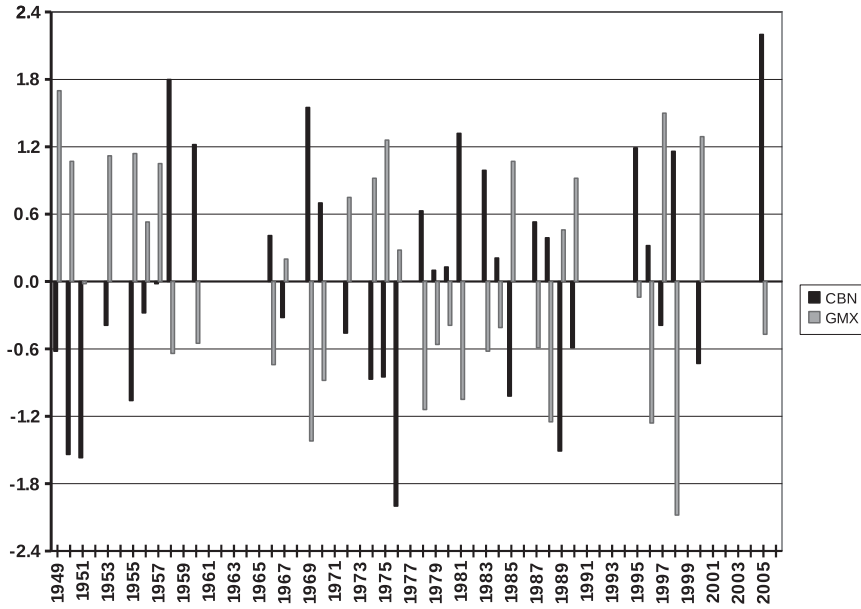
FIG. 1. Time series of standardized SSTAs (°C) averaged over the CBN and the GMX for IAS dipole years. The Caribbean area average is 12°–20°N, 66°–88°W, and the Gulf of Mexico area average is 22°–32°N, 76°–96°W, excluding the Pacific data.

confirms the association with the AMO showing a multidecadal behavior and same-sign anomalies over the North Atlantic in general. The high-pass index shows an SSTA tripole in the North Atlantic (and its corresponding SSTA dipole in the IAS) and large SST anomalies in the tropical Pacific. The North Atlantic high-pass index has a correlation of 0.58 with the Niño-3.4 index when the Niño-3.4 index leads by 2 months. This indicates that the high correlation between the North Atlantic high-pass index and the dipole index shows the intercorrelation with the Niño-3.4. The remote forcings will be discussed in more detail in the following sections. Because there are teleconnections that lead the dipole index we focus on the anomalies of atmospheric

circulation and air–sea fluxes that lead the IAS SST anomalies.

4. Formation of the IAS SSTA dipole

The associated net heat flux anomalies leading the dipole (Fig. 6e) also have a dipole structure with positive (downward) anomalies over the Caribbean and TNA and negative (upward) anomalies over the Gulf of Mexico and eastern coast of the United States. In the Gulf of Mexico, from the turbulent and radiative heat fluxes, the main contributor is the latent heat flux (Fig. 6a). When the latent heat flux is decomposed (see section 2) and its components are regressed onto the dipole index
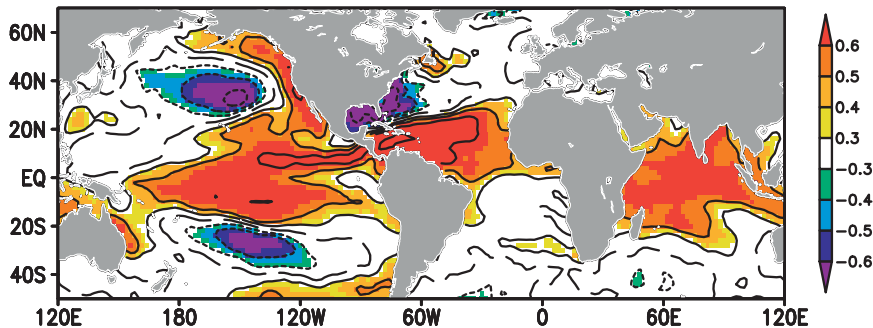

FIG. 2. February–April correlation between the IAS SSTA dipole index and SSTAs (°C) from 1949 through 2006. The contour interval is 0.2 starting at ±0.3. The long-dashed contour is the zero correlation contour.
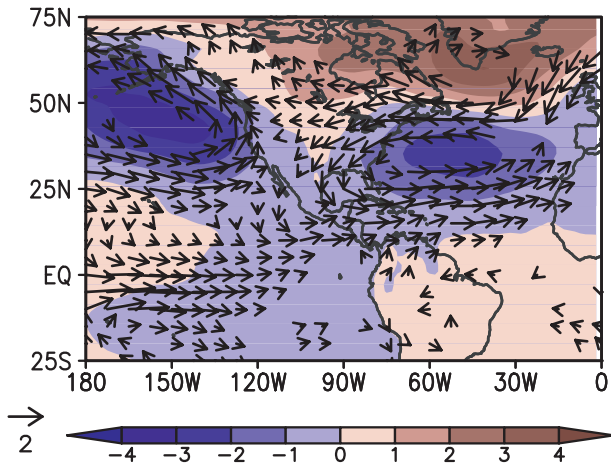
FIG. 3. February–March regression of IAS SSTA dipole index onto 850-hPa wind (m s^{-1}; vectors) and surface pressure (hPa; shades) from 1949 to 2006.

(Table 3), it becomes evident that the component that contributes the most in the Gulf of Mexico is $W\delta q'$. The sensible heat flux also has a large contribution to the SSTA dipole in the Gulf of Mexico region (Fig. 6b), and the term that dominates in the Gulf of Mexico is the $\delta T'$ term. In the Caribbean, the regression values of sensible heat flux are small and neither term dominates. Although it also has small latent heat flux anomalies in the Caribbean, the $W\delta q'$ term contributes the most to the positive latent heat flux anomalies. The $W\delta q'$ contri-

bution in the Caribbean was also found by Chikamoto and Tanimoto (2005) to be significant.

In the Gulf of Mexico the surface winds blow mainly in the meridional direction (Fig. 6f), which coupled to the stronger meridional gradient of humidity renders the $W\delta q'$ component of the latent heat flux as the dominant. Because the northerly wind anomalies north of and in the Gulf of Mexico inhibit the transport of moisture to the continental United States and advect dry air from the north, the air–sea difference in moisture triggers heat fluxes that ultimately cool the SSTs in the Gulf of Mexico. In the IAS during springtime there is also a meridional gradient of SST and surface air tempera-ture. Hence, following the rationale of Cayan (1992), the $\delta q'$ and $\delta T'$ terms have more prominence in the Gulf of Mexico as it is in this region where the wind anomalies are stronger in the meridional direction (Fig. 3).

The correlation between the dipole index and IAS subsurface temperature is significant when the subsurface temperature anomalies lag the dipole index. However, the correlation is not significant when the subsurface temperature anomalies lead the dipole index. The lag of subsurface temperature anomalies indicates that air–sea interactions are the principal conduit by which the IAS is forced during late winter and early spring.

For the case of a higher air–sea moisture difference in the Gulf of Mexico during the IAS SSTA dipoles, the cloudiness increases. This aspect is reflected in the short-wave radiation anomalies (Fig. 6c). Negative shortwave
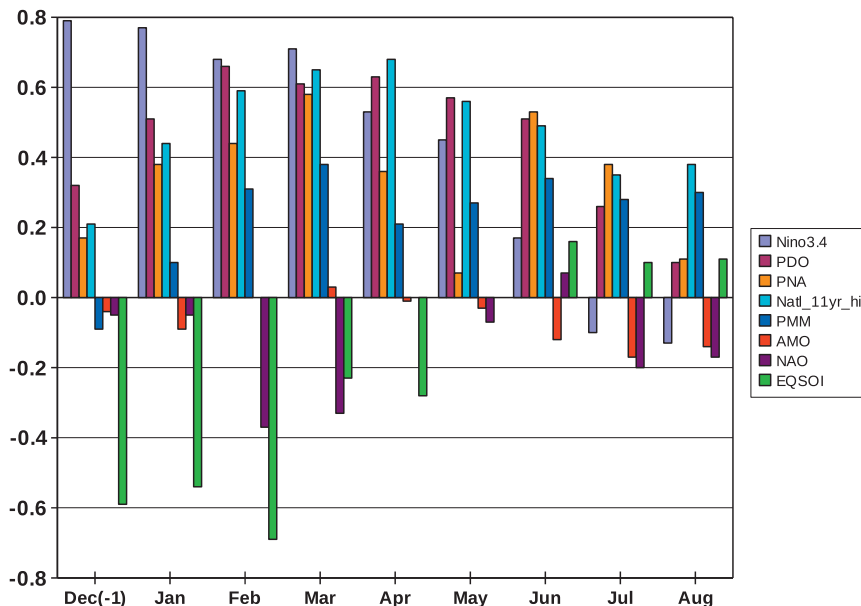

FIG. 4. Correlation between the IAS SSTA dipole index and teleconnection indices in the Pacific (PDO, PNA, Niño-3.4, EQSOI, and PMM) and in the Atlantic (AMO, NAO, national 11-yr high pass).
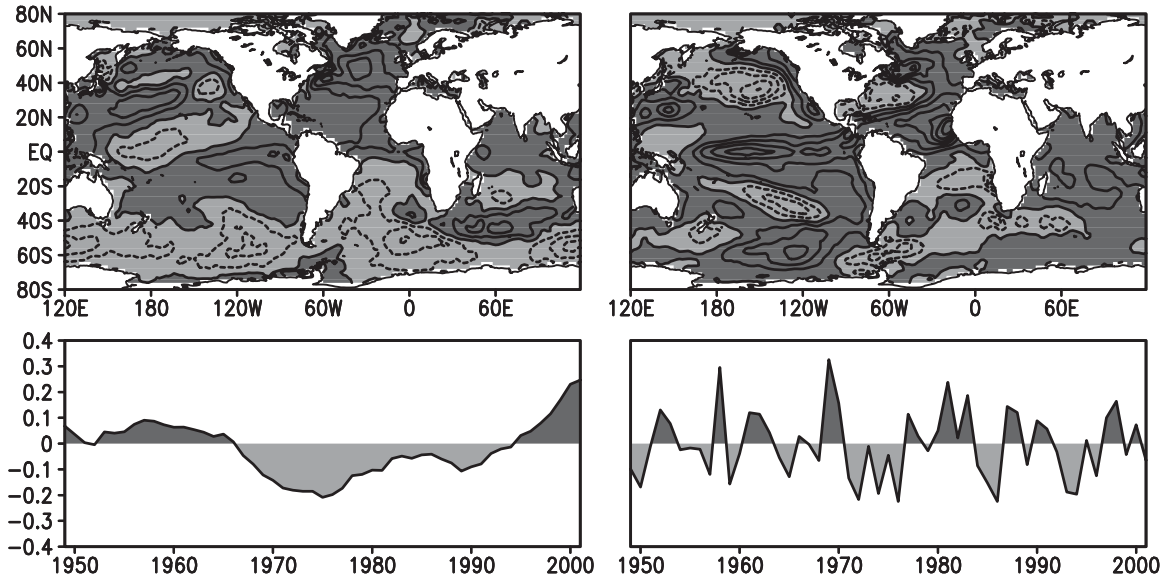
FIG. 5. (top) Regression of SSTA (°C) onto 11-yr (left) low-pass and (right) high-pass North Atlantic SSTA index from 1949 to 2001. Contour interval is 0.1°C. Positive values are in dark gray and solid contours. Negative values are in light gray and dashed contours. (bottom) Time series of the 11-yr (left) low-pass and (right) high-pass index. (See text for explanation of indices.)

anomalies are more prominent over the Gulf of Mexico and western Caribbean and centered near the Yucatan Channel and the Straits of Florida. The increase in cloudiness would in turn cool the surface waters of the Gulf of Mexico because it blocks the shortwave radiation penetration. However, in the western Caribbean Sea this is offset by the increase in longwave radiation. In the eastern Caribbean Sea, the shortwave radiation still penetrates and the latent heat flux also acts to warm the sea. Associated with the surface wind anomalies are downwelling anomalies along the South American coast in the eastern part of the Caribbean (Fig. 6f), which also contribute to the warming of the SSTs.

The negative shortwave anomalies are collocated with an increase in upper-level divergence, indicating an anomalous rising branch in the atmospheric circulation over the IAS (Fig. 7, top). The corresponding anomalous sinking branch lies over the eastern Amazon basin and western deep tropical Atlantic (i.e., 5°S–15°N, 35°–65°W).

5. Teleconnections

a. Divergent circulation

Boreal winter and spring are the seasons when the convection over the Amazon is stronger and closer to the equator (especially during spring). In the climatology, the convection cell has a sinking branch stronger over the TNA and a weaker sinking branch over the IAS. However, when the IAS SSTA dipole index is

regressed on atmospheric circulation fields, the relationship between the Amazon region and the IAS stands out (Fig. 7). Even though there are also divergent wind anomalies connecting the easternmost equatorial Pacific with the Amazon basin, the February–March anomalies of the divergent wind are stronger between the IAS and the Amazon basin (Fig. 7, top). These relationships confirm that the precipitation and convection anomalies over the Amazon region are related to the IAS, in this case the IAS dipole during spring.

Before the mature phase of the IAS dipole in March, the December–January vertical velocity anomalies show an upward anomaly over the IAS (stronger over the northeast of the Greater Antilles). The divergent wind anomalies aloft diverge from that region and converge over northeastern South America (over the eastern Amazon basin) and the western TNA between the equator and 10°N. In those regions there are subsidence anomalies and a decrease in precipitation. At the lower levels, the divergent circulation (not shown) is directed from northeastern South America toward the IAS, closing the circulation cell. The inhibition of convection over the Amazon is also a response to the weakening of the Atlantic trade winds that at this time of the year carry moisture to the Amazon region. By having less humidity in the region, less convection develops.

A separate circulation cell that connects the IAS to the Midwest of the United States develops in February–March. The upward velocity anomaly over the Caribbean has a descending counterpart over the Midwest,
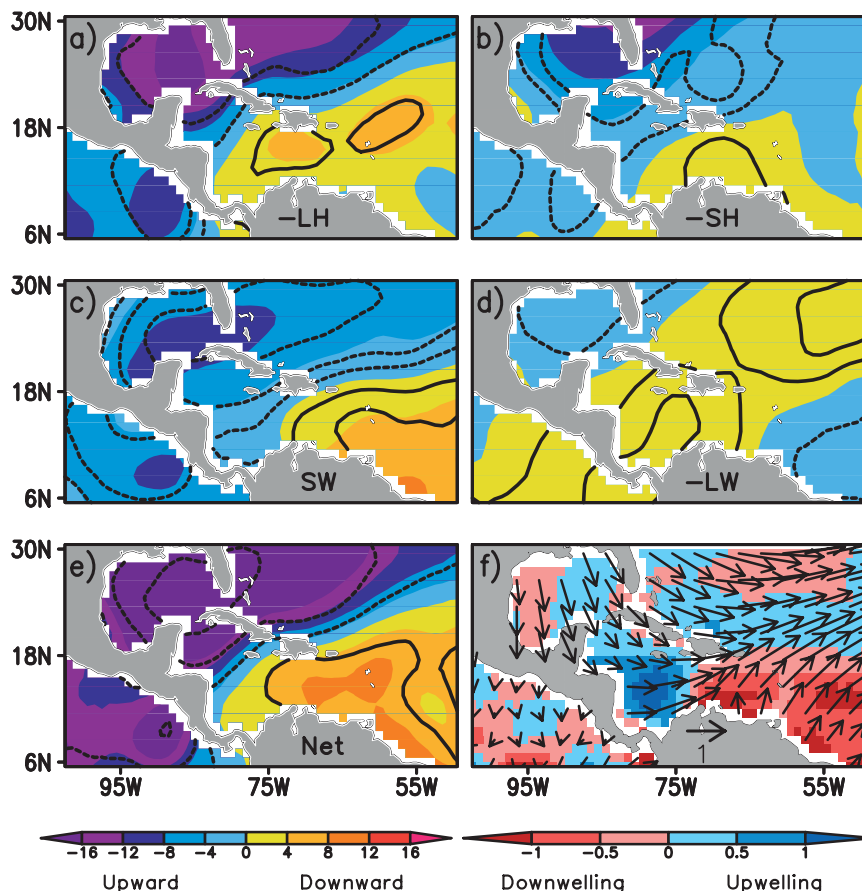
FIG. 6. (a)–(e) January–March average regression (1949–2002) of turbulent and radiative air–sea heat fluxes (W m^{-2}) on dipole index (shades). (a) Latent heat flux, (b) sensible heat flux, (c) shortwave, (d) longwave, and (e) net heat flux. The contours in (a)–(e) indicate the correlation at intervals of 0.2 starting at $\pm$0.2 (negative correlations are shaded and positive correlations are solid). The contours in (e) indicate the $\pm$0.3°C SSTA regression values. (f) The regression of wind stress (arrows; 10^{-2} N m^{-2}) and Ekman pumping (shades; m month^{-1}) is shown. The reference arrow is 1×10^{-2} N m^{-2}.

and strong irrotational wind anomalies diverge from the IAS and converge over the Midwest. In fact, the precipitation over the Midwest region decreases whereas it increases over the Florida peninsula. As we have discussed above, this circulation cell also extends to the lower levels where the irrotational circulation anomalies are in the opposite sense as those aloft. (It is important to remember that the results discussed above come from the regression of the dipole index onto climatic fields and that the dipole index is correlated not only to ENSO but also to other teleconnection patterns.) In fact, the convection anomaly over the IAS may also be related to the low-pressure anomaly of the PNA wave train that reaches the IAS.

b. ENSO versus PNA

To distinguish between the influence of the PNA and that of the equatorial Pacific anomalies on the IAS SST

anomalies, an analysis was done from a sample of the Niño-3.4 index that excludes 20 March extreme events of the PNA index. The March PNA extreme events excluded are the 10 most negative events: 1954, 1955,

TABLE 3. January–March average regression (1949–2002) of components of the turbulent air–sea heat fluxes (W m^{-2}) onto the dipole index. GMX is the Gulf of Mexico area average and CBN is the Caribbean Sea area average. Because these are area averages the components may not balance each other.

Component	GMX	CBN
$W\delta q$	−13.3	2.0
$W\delta q'$	−9.0	3.7
$W'\delta q$	−4.3	−1.7
$W\delta T$	−6.6	0.2
$W\delta T'$	−10.9	−0.3
$W'\delta T$	3.8	0.5

Dec–Jan   Feb–Mar

250hPa Div.Wind, Vel.Pot. & 500hPa Vert.Vel.

Upward   0   Downward

Dec–Jan   Precip.   Feb–Mar

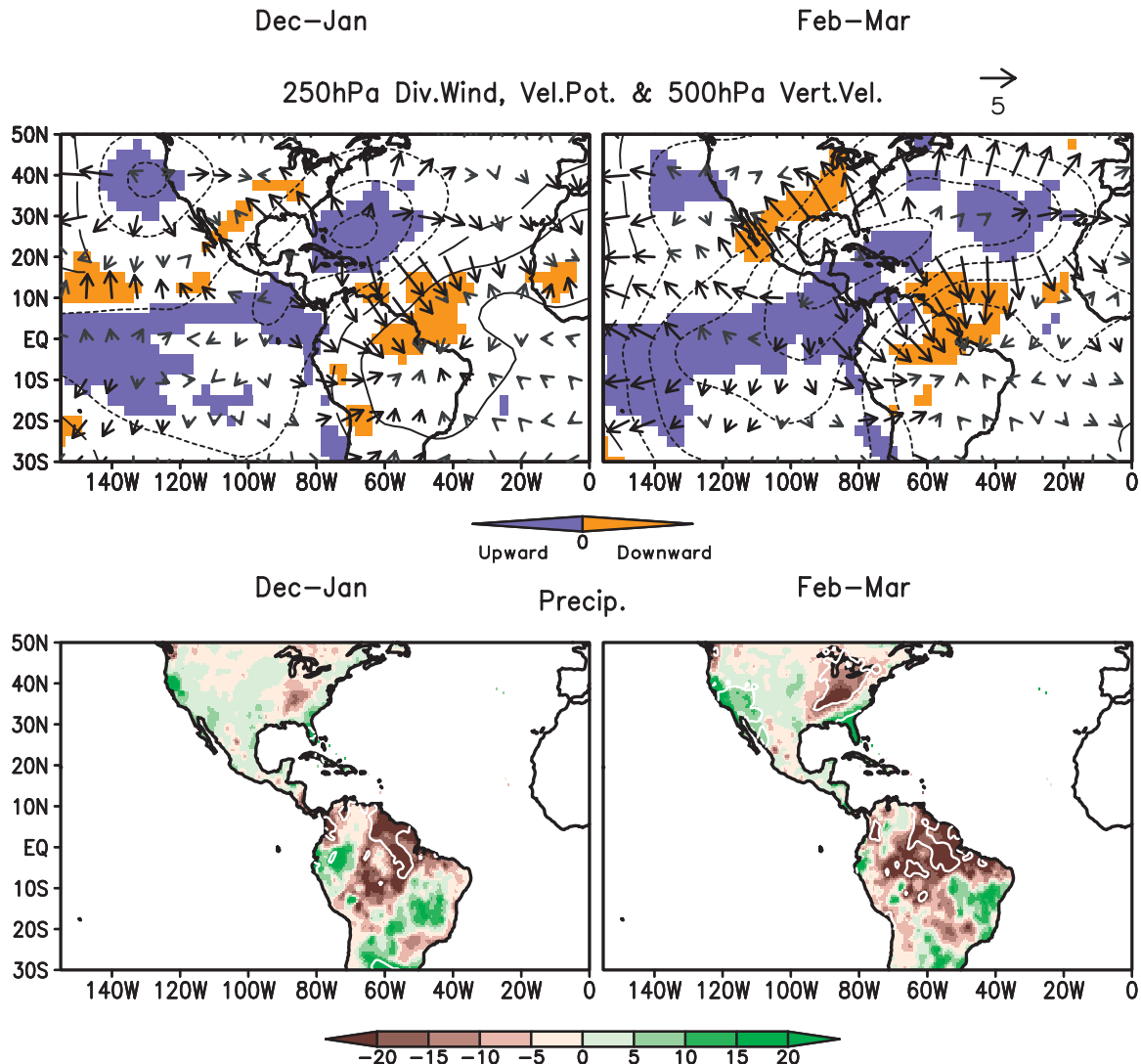
−20 −15 −10 −5   0   5   10   15   20

FIG. 7. (top) Regression of IAS SSTA dipole index onto upper-level (250 hPa) divergent wind (vectors) and velocity potential anomalies (contours). The reference arrow is 10^{-1} m s^{-1}. Black vectors are significant at the 95% level. The shades correspond to where the correlations between the dipole index and the 500-hPa vertical pressure velocity anomalies are greater than 0.3 or less than −0.3. The contour interval for velocity potential is $3\,10^5$ m^2 s^{-1}. (bottom) Regression of precipitation anomalies (mm month^{-1}) with the IAS dipole index. The white contours encompass the regions where the regression is statistically significant at the 95% level.

1963, 1964, 1967, 1976, 1982, 1989, 1997, and 2002; and the 10 most positive events: 1957, 1973, 1981, 1983, 1984, 1986, 1987, 1993, 1998, and 2000. Then, the values of the Niño-3.4 and PDO indices corresponding to those PNA extreme events were removed from their time series to create no-extreme-PNA (no_pna) Niño-3.4 and PDO indices. The no_pna Niño-3.4 index was regressed and correlated to SSTAs in the Atlantic and Pacific basins, as shown in Fig. 8a. For no_pna years the Niño-3.4 index has a positive relation with the Caribbean SSTAs from January, peaking in March and extending across the TNA in April. The Gulf of Mexico SSTAs are not as significantly related to the Niño-3.4, except in February

when the Gulf of Mexico shows cool anomalies as part of a greater area of negative SSTAs that extend to the western North Atlantic region.

The years when the March Niño-3.4 values were extreme were also identified. The 10 yr when the March Niño-3.4 values were the most negative were: 1950, 1951, 1955, 1956, 1971, 1974, 1985, 1989, 1999, and 2000; and the 10 years when the March Niño-3.4 values were the most positive were 1958, 1966, 1969, 1973, 1983, 1987, 1992, 1993, 1998, and 2003. These years were removed from the PNA index and the no-extreme-Niño-3.4 (no_n34) PNA index was analyzed with respect to SSTAs. When there are no extreme Niño-3.4 events in
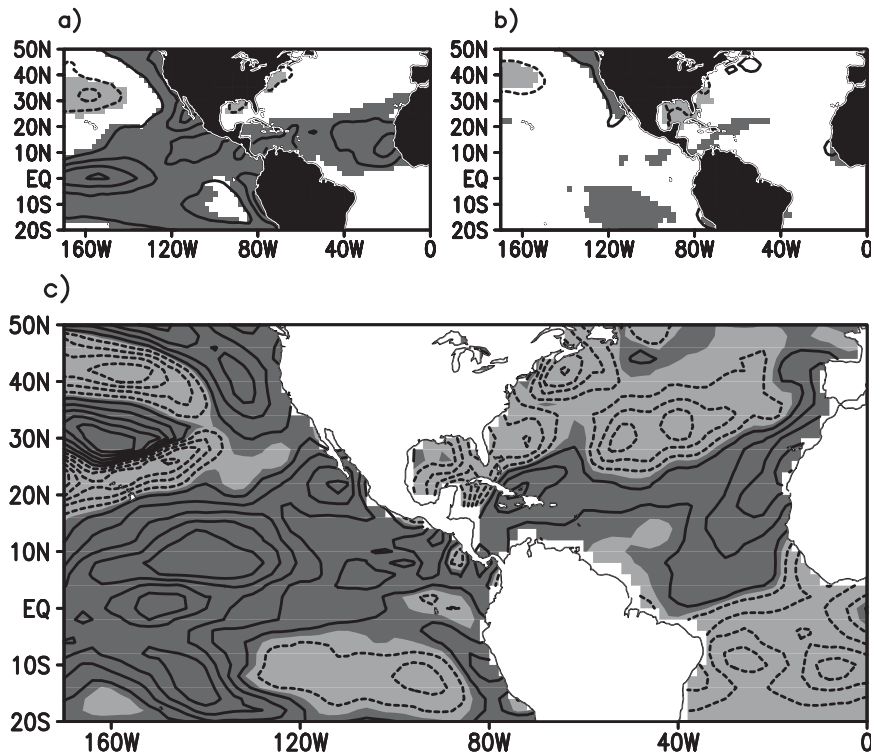
FIG. 8. (a) March–April SSTA (°C) average regression of March Niño-3.4 index when the March PNA extreme years have been excluded. (b) March–April SSTA (°C) average regression of March PNA index when the March Niño-3.4 extreme years have been excluded. Contour interval is 0.2 starting at ±0.2. Values significant at the 95% level are shaded. (c) Difference in explained variance (%) of the March–April partial correlation between the PDO and SSTAs when the PNA index is controlled vs when the Niño-3.4 index is controlled (see text for explanation). Contour interval is 2%. The zero contour has been omitted. Dark gray denotes positive values and light gray denotes negative values.

March, the PNA and PDO indices stay significantly correlated at 0.51. However, the correlation between the Niño-3.4 index and the PNA (and the PDO) drops from 0.48 to 0.19 (from 0.47 to 0.16). Henceforth, the regression of the no_n34 PNA index onto the IAS climate variables has removed some of the ENSO influence on the IAS that is mediated by the PNA. Figure 8b shows the no_n34 PNA index regressed onto SSTAs for the Pacific and Atlantic basins. It can be observed that the PNA influence is mostly on the Gulf of Mexico in March and April. Essentially, during March and April ENSO influences mostly the Caribbean region, and the PNA influences mostly the Gulf of Mexico region. Therefore, when a warm winter–spring ENSO event combines with a positive spring PNA event, the IAS shows a strong dipole of SSTAs with cooler SSTAs in the Gulf of Mexico and warmer SSTAs in the Caribbean Sea and TNA.

The PDO also has a relation to the IAS dipole (Fig. 8c). However, the PDO's relation varies depending on the strength of the PNA and ENSO. To distinguish be-

tween the influence of the PNA and the influence of the Niño-3.4 with respect to the PDO, a comparison was done after calculating the partial correlation of the PDO index and SST anomalies by controlling the PNA index or the Niño-3.4 index. Figure 8c shows the difference in March–April explained variance of the PDO when the PNA is controlled minus when the Niño-3.4 is controlled. It is clear that in the Gulf of Mexico the PDO index has *greater* explained variance when the Niño-3.4 index is controlled versus when the PNA index is controlled. However, in the Caribbean and the TNA the PDO index has *less* explained variance when the Niño-3.4 index is controlled versus when the PNA index is controlled. This, again, indicates a greater association between PNA and the Gulf of Mexico variability, and between Niño-3.4 and the Caribbean Sea variability.

c. Time-scale distinctions

To further explore the remote areas related to the IAS SSTA dipole we apply a 5-yr temporal filter to the
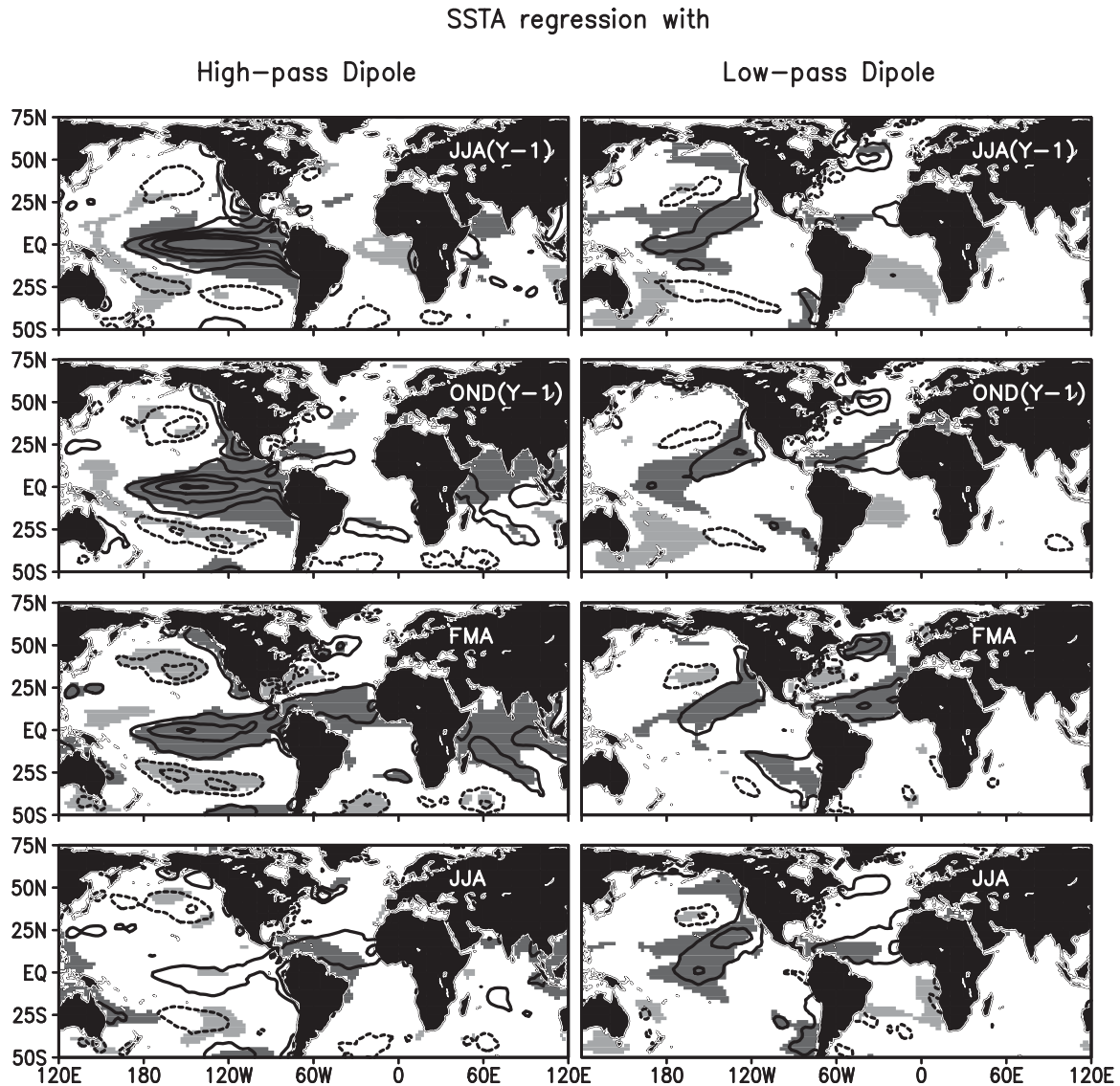
SSTA regression with

FIG. 9. SSTA (°C) regression onto (left) 5-yr high-pass dipole index and (right) 5-yr low-pass dipole index for (from top to bottom) June–August of the previous year, October–December of the previous year, February–April, and June–August. Contour interval is 0.2 starting at ±0.2. Values significant at the 95% level are shaded.

SSTAs and then recalculate the CBN − GMX difference of SSTAs obtaining high-pass and low-pass dipole indices. The 5-yr high-pass dipole variability is strongly related to ENSO tropical Pacific SSTAs (Fig. 9, left column). The tropical Pacific SSTAs correspond to an ENSO event that decays by late spring but that still has significant SSTAs during early spring. The anomalies in the Gulf of Mexico are stronger in March and are significant throughout the spring season until May. However, the Caribbean SSTAs extend longer from January to July. This is probably related to the difference on how the Gulf of Mexico and the Caribbean Sea are forced. The Gulf of Mexico is essentially forced by the meridi-

onal advection of drier air associated with the winter frontal passages occurring across the southern tier of the United States. This variation in storm tracks is mostly in association to Pacific variability during the winter to early spring months. The Caribbean and the TNA respond mostly to the easterly low-level wind anomalies, which have more to do with the NASH and are thus not limited to the early months of the year, but can occur throughout the year. That is, the longer persistence of Caribbean SSTAs is likely due to positive ocean–atmosphere feedback within the tropical Atlantic.

The 5-yr low-pass IAS dipoles are not as strong in the IAS as they are between the oceanic region east of the
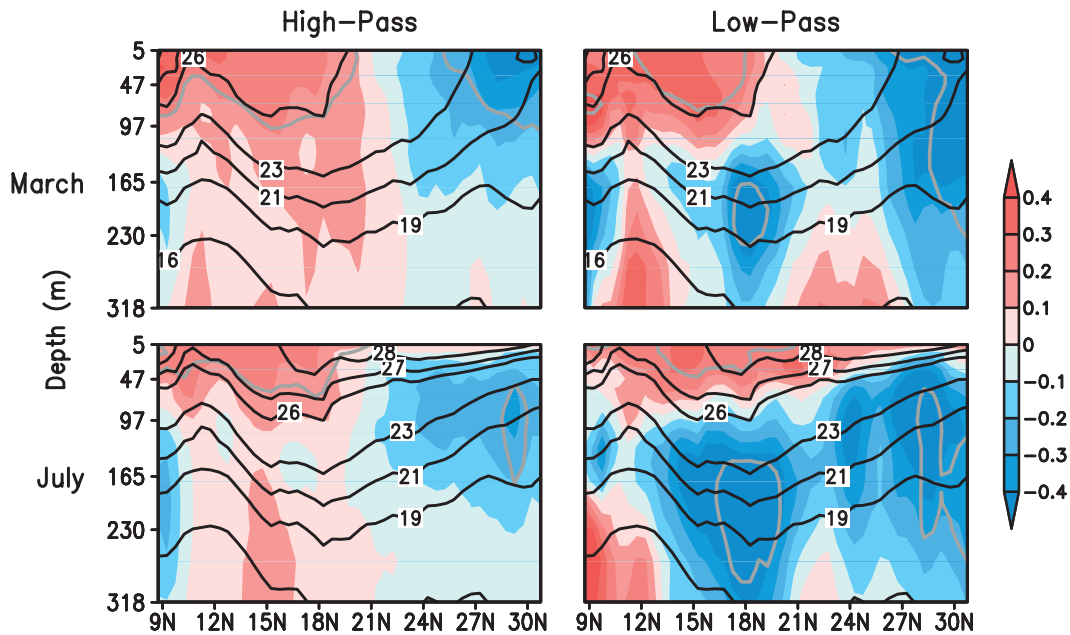
FIG. 10. IAS zonal average of (top) March and (bottom) July regression of subsurface temperature (°C) for the 5-yr (left) high-pass and (right) low-pass IAS spring dipole index. The zonal average is from the western boundary to 60°W. The black contours are the climatological isotherms (°C). The gray contours encompass the depths of significant regressions at the 95% level.

United States and the Caribbean–TNA. Also, they are not related to ENSO anomalies (Fig. 9, right column). They are mostly related to a band of Pacific SSTAs that extends from the subtropical central Pacific to the western coast of the United States. Associated with the development of this band there is also a region of opposing SSTAs to its northwest centered at about 35°N, 160°W. This pattern is similar to the one identified by Chiang and Vimont (2004) as the Pacific meridional mode. In fact, the correlation of the low-pass IAS dipole index and the PMM is 0.55. Also, Paegle and Mo (2002) identified a similar pattern in December–February (Fig. 12d of Paegle and Mo 2002) associated with latitudinal variations of precipitation over South America.

The subsurface temperature anomalies associated with the high- and low-pass IAS dipole indices are shown in Fig. 10. Related to the high-pass dipole the temperature anomalies are consistently warm in the Caribbean basin from the surface to about 300 m. Similarly north of the Caribbean basin the temperature anomalies are consistently cool down to about 200 m. These anomalies extend to the summer season. However, related to the low-pass IAS dipole index the subsurface temperature anomalies are not consistent with depth. The surface warming of the Caribbean extends down to about 100 m. But, farther down there are cool anomalies opposing the surface warming. On the other hand, the cooling north of the Caribbean is consistent with depth and extends to 300 m.

6. Summary and conclusions

Statistical analysis of the variability of SSTAs in the Intra-Americas Sea region during springtime has shown that the IAS has as a main mode of variability an SSTA dipole between the Gulf of Mexico and the Caribbean Sea. Associated with the IAS SSTA dipole are northerly surface wind anomalies that blow from the colder Gulf of Mexico to the warmer Caribbean Sea, and westerly wind anomalies over the Caribbean. This dipole is mainly forced by air–sea turbulent and radiative fluxes with the latent heat flux and the shortwave radiation having the greater influence, with a lead of 2 months. The IAS SSTA dipole is the manifestation of various teleconnections, responding most strongly to the combination of a positive PNA event and a warm ENSO event.

In general, IAS dipole events are established by influences from the midlatitude Pacific and the tropical Pacific. The SSTAs in the Gulf of Mexico are mainly influenced by the PNA and the PDO, whereas those of the Caribbean Sea and the TNA are mainly influenced by ENSO. A warm winter–spring ENSO event reflects as warm SSTAs in the Caribbean Sea and the TNA (Enfield and Mayer 1997; Saravanan and Chang 2000). A positive PNA and positive PDO are both related to cool temperatures in the Gulf of Mexico. The influence of the PNA does not reach as far south in the IAS to

affect the Caribbean Sea SSTs, except when concurrent with warm ENSO conditions.

The contribution of the latent heat flux anomalies in the Gulf of Mexico is mainly due to the air–sea difference in humidity. The air–sea temperature difference is the aspect mostly responsible for the sensible heat flux contribution. The shortwave radiation contribution is a reflection of the changes in cloudiness associated with the dipole. With a cool Gulf of Mexico and a warm Caribbean Sea there is an increase of precipitation over the Gulf of Mexico and the central IAS. The increase of precipitation is related to the air–sea humidity difference because the cold air masses from the north encounter the Gulf of Mexico during positive PNA events and warm ENSO events. The positive anomalies of precipitation over the Gulf of Mexico are also related to a reduced local subsidence, owing to a decrease in convection over tropical South America and western tropical Atlantic. These relationships confirm that the changes in convection and precipitation over the Amazon are strongly linked to the changes in the IAS during late winter and early spring.

A tropical Pacific influence is felt through changes in the regional Hadley circulation that connects tropical South America with the TNA and the IAS. Essentially, as the tropical Pacific warms and the Amazon precipitation diminishes there is a weakening of the meridional overturning (Hadley) cell that connects tropical South America with the IAS–TNA and the NASH. The weakening of this Hadley cell manifests as an increase in precipitation over the IAS (in particular the Gulf of Mexico). The increase in Gulf of Mexico precipitation also has contributions from the air–sea humidity difference (Cayan 1992).

The modulation of the IAS SSTA dipole variability is also influenced by the PDO. The PDO has been described as a low-frequency signal apparently triggered by the white noise from atmospheric phenomena in the Pacific, such as the PNA (Barsugli and Battisti 1998). For the case of the IAS a similar response (i.e., a red oceanic signal as a result of the PNA white atmospheric forcing) may be occurring, and henceforth the correlation of the IAS SSTA dipole with the PDO shows large values (greater than 0.6). Nonetheless, the response of the Gulf of Mexico to atmospheric white noise forcing from the PNA needs to be studied further.

In this study we have demonstrated that in addition to ENSO there are other Pacific teleconnections that influence the IAS climate variability during springtime. This is important with respect to prediction of climate anomalies in the IAS region.

REFERENCES

Alexander, M., and J. Scott, 2002: The influence of ENSO on air–sea interaction in the Atlantic. *Geophys. Res. Lett.,* **29,** 1701, doi:10.1029/2001GL014347.

Barsugli, J. J., and D. S. Battisti, 1998: The basic effects of atmosphere–ocean thermal coupling on midlatitude variability. *J. Atmos. Sci.,* **55,** 477–493.

Carton, J. A., and B. S. Giese, 2008: A reanalysis of ocean climate using SODA. *Mon. Wea. Rev.,* **136,** 2999–3017.

Cayan, D. R., 1992: Latent and sensible heat flux anomalies over the northern oceans: The connection to monthly atmospheric circulation. *J. Climate,* **5,** 354–369.

Chiang, J. C. H., and A. H. Sobel, 2002: Tropical tropospheric temperature variations caused by ENSO and their influence on the remote tropical climate. *J. Climate,* **15,** 2616–2631.

——, and D. J. Vimont, 2004: Analogous meridional modes of atmosphere–ocean variability in the tropical Pacific and tropical Atlantic. *J. Climate,* **17,** 4143–4158.

Chikamoto, Y., and Y. Tanimoto, 2005: Role of specific humidity anomalies in Caribbean SST response to ENSO. *J. Meteor. Soc. Japan,* **83,** 959–975.

Coleman, J. S. M., and J. C. Rogers, 2007: A synoptic climatology of the central United States and associations with Pacific teleconnection pattern frequency. *J. Climate,* **20,** 3485–3497.

Compo, G. P., and P. D. Sardeshmukh, 2004: Storm track predictability on seasonal and decadal scales. *J. Climate,* **17,** 3701–3720.

Curtis, S., and S. Hastenrath, 1995: Forcing of anomalous sea surface temperature evolution in the tropical Atlantic during Pacific warm events. *J. Geophys. Res.,* **100,** 15 835–15 847.

Czaja, A., and C. Frankignoul, 2002: Observed impact of Atlantic SST anomalies on the North Atlantic Oscillation. *J. Climate,* **15,** 606–623.

Deser, C., and M. S. Timlin, 1997: Atmosphere–ocean interaction on weekly time scales in the North Atlantic and Pacific. *J. Climate,* **10,** 393–408.

Dettinger, M. D., D. S. Battisti, G. J. McCabe, C. M. Bitz, and R. D. Garreaud, 2001: Interhemispheric effect of interannual and decadal ENSO-like climate variations on the Americas. *Interhemispheric Climate Linkages,* V. Markgraf, Ed., Academic Press, 1–12.

Eichler, T., and W. Higgins, 2006: Climatology and ENSO-related variability of North American extratropical cyclone activity. *J. Climate,* **19,** 2076–2093.

Enfield, D. B., and D. A. Mayer, 1997: Tropical Atlantic sea surface temperature variability and its relation to El Niño-Southern Oscillation. *J. Geophys. Res.,* **102,** 929–945.

——, A. M. Mestas-Nuñez, D. A. Mayer, and L. Cid-Serrano, 1999: How ubiquitous is the dipole relationship in tropical Atlantic sea surface temperatures? *J. Geophys. Res.,* **104,** 7841–7848.

——, ——, and P. J. Trimble, 2001: The Atlantic multidecadal oscillation and its relation to rainfall and river flows in the continental U.S. *Geophys. Res. Lett.,* **28,** 2077–2080.

——, S.-K. Lee, and C. Wang, 2006: How are large Western Hemisphere warm pools formed? *Prog. Oceanogr.,* **70,** 346–365.

Kalnay, E., and Coauthors, 1996: The NCEP/NCAR 40-Year Reanalysis Project. *Bull. Amer. Meteor. Soc.,* **77,** 437–471.

Klein, S. A., B. J. Soden, and N. C. Lau, 1999: Remote sea surface temperature variations during ENSO: Evidence for a tropical atmospheric bridge. *J. Climate,* **12,** 917–932.

Koren, I., Y. J. Kaufman, L. A. Remer, and J. V. Martins, 2004: Measurement of the effect of Amazon smoke on inhibition of cloud formation. *Science,* **202,** 1342–1345.

Lau, N. C., and M. J. Nath, 2001: Impact of ENSO on SST variability in the North Pacific and North Atlantic: Seasonal dependence and role of extratropical sea–air coupling. *J. Climate,* **14,** 2846–2866.

Lee, S.-K., D. B. Enfield, and C. Wang, 2008: Why do some El Niños have no impact on tropical North Atlantic SST? *Geophys. Res. Lett.,* **35,** L16705, doi:10.1029/2008GL034734.

Lintner, B. R., and J. C. H. Chiang, 2007: Adjustment of the remote tropical climate to El Niño conditions. *J. Climate,* **20,** 2544–2557.

Mantua, N. J., and S. R. Hare, 2002: The Pacific decadal oscillation. *J. Oceanogr.,* **58,** 35–44.

Mestas-Nuñez, A. M., and D. B. Enfield, 2001: Eastern equatorial Pacific SST variability: ENSO and non-ENSO components and their climatic associations. *J. Climate,* **14,** 391–402.

Muñoz, E., A. J. Busalacchi, S. Nigam, and A. Ruiz-Barradas, 2008: Winter and summer structure of the Caribbean low-level jet. *J. Climate,* **21,** 1260–1276.

Nigam, S., 2003: Teleconnections. *Encyclopedia of Atmospheric Sciences,* J. R. Holton, J. Pyle and J. Curry, Eds., Academic Press, 2243–2269.

Okumura, Y., S.-P. Xie, A. Numaguti, and Y. Tanimoto, 2001: Tropical Atlantic air-sea interaction and its influence on the NAO. *Geophys. Res. Lett.,* **28,** 1507–1510.

Paegle, J. N., and K. C. Mo, 2002: Linkages between summer rainfall variability over South America and sea surface temperature anomalies. *J. Climate,* **15,** 1389–1407.

Paeth, H., M. Latif, and A. Hense, 2003: Global SST influence on twentieth century NAO variability. *Climate Dyn.,* **21,** 63–75, doi:10.1007/s00382-003-0318-4.

Rayner, N. A., P. Brohan, D. E. Parker, C. K. Folland, J. J. Kennedy, M. Vanicek, T. Ansell, and S. F. B. Tett, 2006: Improved analyses of changes and uncertainties in sea surface temperature measured in situ since the mid-nineteenth century: The HadSST2 data set. *J. Climate,* **19,** 446–469.

Rodionov, S., and R. Assel, 2001: A new look at the Pacific/North American index. *Geophys. Res. Lett.,* **28,** 1519–1522.

Saravanan, R., and P. Chang, 2000: Interaction between tropical Atlantic variability and El Niño–Southern Oscillation. *J. Climate,* **13,** 2177–2194.

Sciremammano, F., 1979: A suggestion for the presentation of correlations and their significance levels. *J. Phys. Oceanogr.,* **9,** 1273–1276.

Smith, T. M., R. W. Reynolds, T. C. Peterson, and J. Lawrimore, 2008: Improvements to NOAA's historical merged land–ocean surface temperature analysis (1880–2006). *J. Climate,* **21,** 2283–2296.

Straus, D. M., and J. Shukla, 2002: Does ENSO force the PNA? *J. Climate,* **15,** 2340–2358.

Tanimoto, Y., and S.-P. Xie, 2002: Inter-hemispheric decadal variations in SST, surface wind, heat flux and cloud cover over the Atlantic Ocean. *J. Meteor. Soc. Japan,* **80,** 1199–1219.

Trenberth, K. E., G. W. Branstator, D. Karoly, A. Kumar, N.-C. Lau, and C. Ropelewski, 1998: Progress during TOGA in understanding and modeling global teleconnections associated with tropical sea surface temperatures. *J. Geophys. Res.,* **103,** 14 291–14 324.

Wallace, J. M., and D. S. Gutzler, 1981: Teleconnections in the geopotential height field during the Northern Hemisphere winter. *Mon. Wea. Rev.,* **109,** 784–812.

Wang, C., 2002: Atlantic climate variability and its associated atmospheric circulation cells. *J. Climate,* **15,** 1516–1536.

——, 2004: ENSO, Atlantic climate variability, and the Walker and Hadley circulations. *The Hadley Circulation: Present, Past, and Future,* H. F. Diaz and R. S. Bradley, Eds., Kluwer Academic, 173–202.

——, S.-P. Xie, and J. A. Carton, 2004: A global survey of ocean-atmosphere interaction and climate variability. *Earth's Climate: The Ocean-Atmosphere Interaction, Geophys. Monogr.,* Vol. 147, Amer. Geophys. Union, 1–19.

——, W. Wang, D. Wang, and Q. Wang, 2006: Interannual variability of the South China Sea associated with El Niño. *J. Geophys. Res.,* **111,** C03023, doi:10.1029/2005JC003333.

——, S.-K. Lee, and D. B. Enfield, 2008: Climate response to anomalously large and small Atlantic warm pools during the summer. *J. Climate,* **21,** 2437–2450.

Willmott, C. J., and K. Matsuura, 2007: Terrestrial precipitation: 1900-2006 gridded monthly time series (version 1.01). Center for Climatic Research, Department of Geography, University of Delaware. [Available online at http://climate.geog.udel.edu/~climate/html_pages/Global_ts_2007/README.global.p_ts_2007.html.]

Woodruff, S. D., R. J. Slutz, R. L. Jenne, and P. M. Steurer, 1987: A Comprehensive Ocean-Atmosphere Data Set. *Bull. Amer. Meteor. Soc.,* **68,** 1239–1250.